Histological, Fluorescence and Ultrastructural Assessment of Presumptive Effect of Carbimazole Treatment and its Co-administration with Bone Marrow-Derived Mesenchymal Stem Cells on Parotid Glands of Albino Rats

Original Article

Esraa G. Hassan[1]; Heba El Adawy[2] and Amany A. Rabea[1]

[1]Department of Oral Biology, Faculty of Oral and Dental Medicine, Future University in Egypt, Cairo, Egypt

[2]Department of Oral Biology, Faculty of Dental Medicine (Girls), Al Azhar University, Cairo, Egypt

ABSTRACT

Background: Carbimazole is a popular drug for hyperthyroidism. However, it has many side effects on different tissues. Bone marrow-derived mesenchymal stem cells (BM-MSCs) are efficient in tissue regeneration.

Aim: To appraise the consequence of carbimazole (antithyroid drug) intake on albino rat parotid gland structure and plausible outcome of bone marrow-derived mesenchymal stem cells (BM-MSCs) application at different durations.

Material and Methods: Forty adult male albino rats were used and categorized into: Group I: obtained distilled water. Group II: acquired therapeutic dose of carbimazole. Group III: received carbimazole and single dose of BM-MSCs at the start of experiment. Group IV: got carbimazole then by finishing of 3rd week they received solitary injection of BM-MSCs. Preparation of specimens for examination by light, fluorescent and transmission electron microscope was performed. Histomorphometric data of acini area% was statistically analyzed using ANOVA test.

Results: Both histological and ultrastructural examinations illustrated that parotid gland has normal structure in Group I and approximately normal features in Group III. Group II demonstrated distorted acini and duct system. Group IV presented normal features in some acini and some areas of duct system but degenerative features in others. Results of fluorescence labeling explored some labeled-BM-MSCs in Group III but apparently copious labeled cells in Group IV. Statistical results showed highest mean acini area% in Group I, subsequently Group III, then Group IV, followed by Group II.

Conclusions: Carbimazole has deteriorative outcomes on the parotid gland of albino rats. BM-MSCs ameliorate the damaging upshot of carbimazole in a direct proportion manner with time factor.

Received: 10 April 2021, **Accepted:** 05 May 2021

Key Words: BM-MSCs; carbimazole; fluorescent microscope; parotid salivary glands; ultrastructure; .

Corresponding Author: Amany Ahmed Rabea, PhD, Department of Oral Biology, Faculty of Oral and Dental Medicine, Future University in Egypt, Cairo, Egypt, **Tel.**: +2 02 2470 8523, **E-mail:** amanyrabea1@gmail.com

ISSN: 1110-0559, Vol. 45, No.2

INTRODUCTION

Adult parotid gland is the largest major pure serous salivary gland[1]. It has great importance as stimulated parotid gland contributes to total salivary secretion by more than 50% which aids enormously in lubrication of oral cavity and maintenance of its homeostasis together with oral breakdown of carbohydrates[2,3].

Antithyroid drug "carbimazole" is the drug of choice to treat hyperthyroidism. It is a pro-drug that is converted to the active form methimazole after ingestion[4]. It was reported that thyroid hormones decreased after 2, 4 and 6 weeks of treatment by carbimazole[4,5].

Degeneration of prostatic acinar epithelial cells and destruction of hepatocytes were recorded after administration of carbimazole in rats[4,6]. Hyalinization of pancreatic acinar cytoplasm, depletion of pancreas zymogen granules and cytoplasmic organelles, as well as degenerated connective tissue were consequences of treatment by carbimazole[7].

Cell-based therapy is the principle of regenerative medicine exploited in treatment of destructive diseases[8]. Bone marrow-derived mesenchymal stem cells (BM-MSCs) are efficient in tissue regeneration and repair[9,10]. Many studies confirmed that BM-MSCs aid in repair and participate in regeneration of salivary glands[9,11].

Until now, no studies were conducted to analyze the possible effect of carbimazole on salivary glands. So, this study was conducted to evaluate the histological structure of parotid salivary gland throughout treatment by carbimazole and the presumable effect of BM-MSCs at different time spans.

 DOI: 10.21608/ejh.2021.71830.1460

MATERIALS AND METHODS

Isolation and culture of BM-MSCs

Four male albino rats (10 weeks old) were utilized to obtain BM-MSCs. The process was performed at Biochemistry and Microbiology Unit, Faculty of Medicine, Cairo University. Dulbecco's modified Eagle's medium supplemented with 10% fetal bovine serum (GIBCO™/ BRL, USA), was used to flush out bone marrow cells from rats' tibias. Bone marrow cells were centrifuged to obtain mononuclear cell layer which was washed twice in phosphate buffered saline and then centrifuged. Isolated BM-MSCs were cultured in complete culture medium (GIBCO™/BRL, USA) then incubated in 5% CO2 incubator (Innova® CO-170, UK) upon formation of large colonies (80-90% confluence). Washing of cultures twice was performed using phosphate buffered saline and then they were detached using 0.25% trypsin-ethylenediamine tetra-acetic acid, (GIBCO™/BRL, USA). The suspension then centrifuged and cells were resuspended in serum-supplemented medium and inverted phase-contrast light microscope (Olympus®, Tokyo, Japan) was used to monitor the cells at 200x magnification. First-passage cultures were obtained however; the cells used in the experiment were those after the third passage. BM-MSCs cells are spindle shaped. By using Florescent Analysis Cell Sorting (Beckman Coulter®, USA), the cells found to be positive for CD105 and CD29 but negative for CD34[12,13]. Red PKH26 fluorescent linker dye with 551nm excitation and 567nm emission was used to label BM-MSCs cells[14].

Animals

For current study, forty adult male albino rats (180–200gm) were utilized. They were attained from breeding colony, Faculty of Medicine, Cairo University. The animals were numbered and homed in metallic cages (5 rats/each) in proper environment (light/dark cycle, controlled temperature and humidity, as well as proper ventilation) and supplied with water and ground barely ad-libitum. Approval of Animal Ethics Committee, Al-Azhar University (approval number: REC18-081) was verified for animal procedures.

One week was set as acclimatization period. Afterwards, random division of animals into four groups was performed (10 rats/group) as follows:

Group I (Control negative group): the rats received by intra-gastric intubation distilled water as vehicle (5ml/kg b.wt/day) for 6weeks[15].

Group II (Control positive group): carbimazole (Neo-Mercazole® 5mg, Amdipharm Mercury, Australia) was administrated to rats in therapeutic dose (1.35mg/kg b.wt/once/day) after dissolving it in 5ml distilled water via intra-gastric intubation for 6weeks[16].

Group III (6 weeks BM-MSCs treatment): simultaneously, carbimazole was administrated as mentioned previously and at beginning of its administration single dose of BM-MSCs (1x107) in 1ml phosphate buffered saline was injected in tail vein of each rat under anesthesia by ether inhalation[14].

Group IV (3 weeks BM-MSCs treatment): administration of carbimazole was performed as previously mentioned. Each rat at the end of 3rd week received BM-MSCs by single injection as mentioned previously[14].

Animals sacrifice

At the end of 6th week (experimental period), euthanasia was performed for all animals by over dose of ketamine[17].

Parotid glands dissection

The parotid salivary glands of the left and right sides were dissected from each numbered rat. The surrounding fat tissue and lymph nodes were removed carefully from the glands. The gland of each side for each rat was placed in numbered and labeled plain vacutainer (Voma Med® 5ml, Turkey). Numbering and labeling of each vacutainer were according to the rat's number and gland's direction in rat, to facilitate comparing results of different examination modalities of the same rat. Glands of right side were immediately fixed in 10% neutral buffered formalin to be prepared for histological staining and for examination of labeled cells by fluorescence microscope[17]. Glands of left side were segmented into cubes (1mm3), then fixation of specimens in 2.5% glutaraldehyde buffered with 0.1mol phosphate buffer at pH 7.4 was achieved at 4°C for 2h to be examined by transmission electron microscope[18].

Specimen preparation

Gland portions immediately fixed in 10% neutral buffered formalin were remained for 48h in the fixative. Tap water was used to wash the specimens, ascending grades of ethyl alcohol was utilized for dehydration, xylene and paraffin wax were used for clearing and embedding of specimens respectively[17]. Sections of about 5µm thickness were prepared and segregated into 2 sets. 1st set was prepared for routine hematoxylin and eosin (H&E) staining. 2nd set was left unstained for examination of PKH26-labeled cells.

Both sets were deparaffinized in xylene, then rehydrated in descending ethanol series ending by H_2O[17].

H&E staining

To explore histological details of parotid glands, H&E solutions (Sigma®, St. Louis, USA) were used for histological staining[19].

The histological sections were examined by inverted light microscope (Olympus®, BX40F4, Japan). Both terminal secretory units and duct system were photographed at 400x magnification.

Preparation for detection of PKH26-labeled cells

The unstained sections were examined by fluorescence Microscope (Leica®, D-35578, Germany) to detect

cells labeled by PKH26 to ensure their engraftment into parotid glands. The sections were photographed at 400x magnification.

PKH26 was used to label BM-MSCs as it is simple labeling procedure. Beside, PKH26 is stable till 4 months and it does not affect neither cell's function nor its proteins[20,21].

Preparation for transmission electron microscope

Glands of left side (1mm^3) fixed in 2.5% glutaraldehyde buffered with 0.1mol phosphate buffer (pH 7.4) for 2h at 4°C, were fixed furthermore for 1h in 1% osmium tetroxide in same buffer. Afterwards, dehydration and embedding in epoxy resin then polymerization at 60°C for 24h were carried out. Ultra-microtome (Lecia Ultra-Cut®, UK) was used to obtain both semithin and ultrathin sections. Semithin sections were stained by toluidine blue to select areas to be ultrathin sectioned. Ultrathin sections were collected on copper grids then stained by uranyl acetate and lead citrate[18]. Terminal secretory units as well as duct system were examined and photographed at 8,000× − 40,000× magnifications by using transmission electron microscope (JEOL JEM® 1010, Jeol Ltd, Japan). This was performed at Regional Center of Mycology and Biotechnology (RCMB), Al-Azhar University, Egypt.

Histomorphometric analysis

To assess area% of acini, histomorphometric analysis of histological sections was done utilizing ImageJ software (version 1.8.0; NI H, USA). Calibration of the image analyzer automatically was performed at first for conversion of program measurement units (pixels) into actual micrometer units. Regarding each specimen, the analysis was performed for seven fields at 400x magnification. Grey calibration was done to obtain grey delineated image to select areas showing acini. Then blue binary color was used to mask the selected areas. Then obtaining of mean values for each specimen was attained. The analysis was performed relative to standardized measuring frame area (120,000 μm^2).

Statistical analysis

Statistical presentation of obtained histomorphometric data was in form of mean values ± standard deviation (±SD). For comparing the different studied groups, One-way ANOVA test was utilized and when it showed statistical significance it was consequently followed by post hoc test "Least Significant Difference". Significant results were indicated by probability value (*P-value*) ≤ 0.05 while, highly significant results were indicated by *P-value* < 0.001. Statistical Package for the Social Sciences 20 (SPSS® Inc., Chicago, USA) was used in statistical analysis.

RESULTS

Histological results

Group I (Control negative group)

Examination of Group I histological sections revealed that the glands were divided into lobes and lobules by connective tissue septa. Serous acini formed terminal secretory units of the gland. The acini were spherical consisting of pyramidal cells where their apices surrounded apparently narrow central lumen. Cells' apices were eosinophilic and cytoplasm was moderately basophilic with spherical basal ap¬parently large nu¬clei. Myoepi¬thelial cells' flattened nuclei were observed embracing some acini and intercalated ducts. Intercalated ducts were lined by cuboidal cells their cytoplasm was basophilic with apparently large central rounded nuclei. The ducts' lumina were apparently large relative to those of acini. Blood vessels with normal endothelial lining were detected (Figure 1a). Striated ducts were lined by columnar cells. The lining cells showed eosinophilic cytoplasm with well-defined eosinophilic basal striations and centrally located nuclei. The lining cells surrounded apparently regular and wide lumen (Figure 1b). Obviously large excretory ducts were lined by pseudostratified columnar epithelium. Their lumina seemed to have variable diameters. Dense connective tissue with regular collagen fiber bundles surrounded the ducts and adjacent blood vessels with normal endothelium were noticed (Figure 1c).

Group II (Control positive group)

Histological examination of Group II explored noticeable shrinkage in acini size as well as perceptible decrease in their number. Some acini were degenerated. Most of acini were distorted with ill-defined cellular outline, cytoplasmic vacuolations, loss of cytoplasmic basophilia and loss of cells' apices eosinophilia. Pyknotic, pleomorphic, hyperchromatic and karyolitic nuclei were detected in most cells. Among acini; desquamated cells, spacing, extravasated red blood cells and congested blood vessels engorged with red blood cells were detectable. Myoepithelial cells exhibited pyknotic nuclei. Intercalated duct cells showed apparent loss of height, scanty cytoplasm, hyperchromatic and pyknotic nuclei. Cytoplasmic vacuolations were noticed in some ductal cells. Observable dilated duct lumen was noticed. Striated duct cells evidently lost both their height and their basal striations in addition to presence of cytoplasmic vacuolations. Some of their nuclei were karyolitic, and others were pyknotic and hyperchromatic (Figure 2a). Excretory ducts epithelial lining lost its pseudostratification. Most of ductal cells showed karyolitic, hyperchromatic and pyknotic nuclei. Some duct cells showed cytoplasmic vacuolations. The duct lumen illustrated stagnated secretion. Areas of degeneration, hyalinization, disorganized collagen fiber bundles, inflammatory cells infiltration as well as dilated and congested blood vessels were noticed in the surrounding connective tissue (Figure 2b).

Group III (6 weeks BM-MSCs treatment)

Histological examination of Group III showed more or less normal histological features of parotid gland. Connective tissue septa divided the glands into lobes and lobules. Noticeably normal sized spherical acini showed apparently high pyramidal cells having moderately basophilic cytoplasm and deeply stained basophilic rounded basal nuclei. The acinar cells encircled distinctly narrow lumen. Perceptibly very few degenerated acini were detected. Apparently large blood vessels and markedly few extravasated red blood cells were observed. Flattened nuclei of myoepi¬thelial cells could be noticed. Intercalated ducts were lined by cuboidal cells their cytoplasm was basophilic and having centrally apparently large spherical nuclei. Lumina of the ducts were patently larger than those of acini. Most of striated duct cells were columnar with central nuclei, eosinophilic basal striations and acidophilic cytoplasm. However, obviously few ductal cells showed apparent loss of both cell height and basal striations (Figure 3a). Pseudostratified columnar epithelium lined excretory ducts except for manifestly few small areas of duct lining where loss of pseudostratification was noticed. Apparently wide patent lumen was observed. Regular collagen bundles of dense connective tissue surrounded the ducts except for apparently small areas of hyalinization. Markedly few scattered inflammatory cells were detected. Blood vessels with normal endothelial lining were observed (Figure 3b).

Group IV (3 weeks BM-MSCs treatment)

Histological examination of Group IV showed that most of acini were strikingly normal sized and spherical in shape with conspicuously narrow lumen. Many of acinar cells were manifestly high pyramidal cells with basally situated deeply basophilic rounded nucleus and moderately basophilic cytoplasm. However, apparently few acini seemed to be shrunken with ill-defined cell outline. Some acinar cells had karyolitic, pyknotic, pleomorphic and hyperchromatic nuclei as well as cytoplasmic vacuolations. Discernibly small areas of degenerated connective tissue septa were observed. Perceptibly small blood vessels and extravasated red blood cells were detected among acini. Spindle shaped nuclei of myoepi¬thelial cells could be noticed. Most of intercalated duct cells were cuboidal and had distinctly large spherical nucleus and basophilic cytoplasm. But apparently few ductal cells were obviously reduced in height. The ducts' lumina were evidently larger than those of acini. Some of striated duct cells were columnar with central nuclei, basal eosinophilic striations and eosinophilic cytoplasm. However, some cells of striated ducts showed marked loss of height, pyknotic nuclei and loss of basal striations (Figure 4a). Some areas of excretory duct epithelial lining were pseudostratified columnar epithelium while, other areas showed loss of pseudostratification and apparently few pyknotic nuclei were spotted. The duct had plainly wide and patent lumen. Some areas of dense connective tissue surrounding excretory ducts showed regularly arranged collagen bundles, while other areas of hyalinization and inflammatory cells infiltration were detected. Obviously small areas of degeneration were perceived. Blood vessels were congested and engorged by red blood cells. Lymphatic vessels were dilated as well (Figure 4b).

Fluorescence labeling results

PKH-26 labeled-BM-MSCs appeared as red fluorescent cells. Group III demonstrated some labeled-BM-MSCs (Figure 5a). Obviously numerous labeled-BM-MSCs were illustrated in Group IV (Figure 5b).

Ultrastructural results

Group I (Control negative group)

Group I revealed acinar cells' nuclei were apparently large with dispersed loose chromatin, and condensed chromatin attached to nuclear membrane. Apparently variable sized, spherical zymogen granules with high electron-density were detected. The acinar cells were attached together by junctional complexes (Figure 6a). Well-defined rough endoplasmic reticulum cisternae were arranged basally (Figure 6b). Zymogen granules were delineated by explicit membrane. Distinct Golgi complex saccules were situated apical and lateral to the nucleus. Mitochondria with definite cristae were erratically distributed (Figure 6c). The cuboidal intercalated duct cells showed obviously large nuclei most of their condensed chromatin attached to nuclear membrane while some condensed chromatin were dispersed within loose chromatin. Noticeably small highly electron-dense apical secretory granules were noticed. Regular duct lumen was illustrated (Figure 7a). Unambiguous rough endoplasmic reticulum cisternae as well as mitochondria with remarkable cristae were observed. Secretory granules were bounded by delineating membrane. The duct cells were joined by scattered desmosomes and apical junctional complexes (Figure 7b). Striated duct cells showed deeply folded basal plasma membrane and alternating vertically arranged elongated mitochondria with well-defined cristae. Distinct cisternae of rough endoplasmic reticulum were detected (Figure 7c). Definite junctional complexes and tight junctions were noticed joining adjacent cells (Figure 7d). Cytoplasm of excretory duct cells showed membrane bounded highly electron-dense secretory granules. Distinctive rough endoplasmic reticulum cisternae and mitochondria with idiosyncratic cristae were observed. Junctional complexes and desmosomes were detected between duct cells (Figure 7e). The barrel shaped Goblet cells showed nucleus with condensed chromatin and cytoplasm filled by electron-lucent mucous secretory granules (Figure 7f).

Group II (Control positive group)

Group II showed cells of acini had nuclei with condensed chromatin attached to nuclear membrane and dispersed also widely within loose chromatin. Apparently widened intercellular canaliculi and loss of intercellular

junctions were noticed. Some acinar cells showed areas of dilated rough endoplasmic reticulum cisternae (Figure 8a). Some of acini cells showed degenerated rough endoplasmic reticulum. Obvious different sized zymogen granules were observed. Most of granules had low electron-density and noticeably few granules were moderately electron-dense (Figure 8b). Most of zymogen granules exhibited ill-defined membrane. Dilated saccules of Golgi apparatus and degenerated swollen mitochondria with ill-defined cristae were detected (Figure 8c). Intercalated duct cells displayed pyknotic and karyolitic nuclei as well as many nuclei with irregular outline. Apparently few secretory granules with different electron densities were noticed. Perceptibly large cytoplasmic vacuolations and irregular duct lumen were demonstrated (Figure 9a). Fragmented rough endoplasmic reticulum and degenerated mitochondria were revealed. Secretory granules lacked a definite bounding membrane. Lack of most intercellular junctions as well as noticeably wide intercellular spaces were observed (Figure 9b). Striated duct cells showed apparent loss of height, irregular outline and very shallow basal plasma membrane infoldings with apparently short degenerated mitochondria. Crumbled rough endoplasmic reticulum was illustrated (Figure 9c). Manifestly wide intercellular spaces and evidently few intercellular junctions were demonstrated (Figure 9d). Excretory duct cells represented low electron-dense secretory granules with ill-defined boundaries. Both rough endoplasmic reticulum and mitochondria were degenerated. Ill-defined intercellular junctions were recognized as well (Figure 9e). Goblet cells had indistinct outline, karyolitic nuclei and devoid of mucous secretory granules (Figure 9f).

Group III (6 weeks BM-MSCs treatment)

Group III demonstrated nuclei of acinar cell were noticeably large with nuclear membrane had attached condensed chromatin and prominent nucleoli within dispersed loose chromatin. Spherical zymogen granules with apparent different sizes were noticed. Some granules showed high electron-density, others were moderately electron-dense and few had low electron-density. Intercellular junctions were noticed in some areas however, other areas showed absence of intercellular junctions and manifestly widened intercellular canaliculi. Rough endoplasmic reticulum with well-defined cisternae was arranged basally (Figure 10a). Most of zymogen granules had well-defined boundaries and surrounded by recognizable membrane but few granules exhibited ill-defined delineating membrane. Most of mitochondria had definite cristae. However, few mitochondria were degenerated (Figure 10b). Characteristic flattened Golgi complex saccules were observed (Figure 10c). Cells of intercalated ducts revealed markedly large nuclei with prominent nucleoli located within dispersed loose chromatin and nuclear membrane showed attached condensed chromatin. Apparently variable sized highly electron-dense secretory granules were located apically. Almost regular duct lumen was detected (Figure 11a). Rough endoplasmic reticulum cisternae were definite and mitochondria with their notable cristae were demonstrated. The secretory granules boundaries were demarcated by delineating membrane. Junctional complexes and desmosomal junctions were detected (Figure 11b). Cells of striated ducts showed somewhat deep infoldings of basal plasma membrane with alternating mitochondria which had well-defined cristae and arranged vertically. Some of mitochondria in basal infoldings were elongated however, others were ovoid in shape. Characteristic rough endoplasmic reticulum cisternae were noticed (Figure 11c). Remarkable tight junctions and junctional complexes were illustrated between duct cells (Figure 11d). Secretory granules with high electron-density and bordered by definite membrane were detected in excretory duct cells' cytoplasm. Mitochondria with distinctive cristae and characteristic rough endoplasmic reticulum cisternae were noticed. Intercellular desmosomal junctions and junctional complexes were demonstrated (Figure 11e). Barrel shaped Goblet cells showed nuclei with both condensed and loose chromatin. The cell's cytoplasm illustrated some electron-lucent mucous secretory granules as well as some secretory granules ranged from moderately to highly electron-dense (Figure 11f).

Group IV (3 weeks BM-MSCs treatment)

Group IV illustrated acinar cells' nuclei were apparently large with attached condensed chromatin to nuclear membrane and prominent nucleoli present in dispersed loose chromatin. Noticeably variable sizes of spherical zymogen granules were detected. Some granules illustrated low electron-density while others were moderately electron-dense. Intercellular junctions were exemplified in apparently few areas and many areas were devoid of intercellular junctions with markedly widened intercellular canaliculi. Well-defined cisternae of rough endoplasmic reticulum were arranged basally yet, apparently few areas showed dilated cisternae (Figure 12a). Some zymogen granules displayed ill-defined bounding membrane while other granules' boundaries were delineated by recognizable membrane. Some mitochondria showed definite cristae while others were degenerated. Golgi apparatus saccules were flattened except for obviously few saccules that appeared dilated (Figure 12b). Intercalated ducts' cells showed obviously large nuclei with condensed chromatin attached to nuclear membrane and prominent nucleoli within dispersed loose chromatin. Noticeably variable sized secretory granules were detected. Some were highly electron-dense while others had moderate electron-density. Somewhat irregular duct lumen was observed (Figure 13a). Rough endoplasmic reticulum with distinct cisternae was observed except, few cisternae of rough endoplasmic reticulum were fragmented. Mitochondria with remarkable cristae were observed. Membrane bounded secretory granules were recognized. Some intercellular areas showed intercellular junctions but other areas were devoid of intercellular junctions and showed markedly wide intercellular spaces (Figure 13b). Striated duct cells

exhibited extremely shallow basal plasma membrane infoldings nevertheless, the basally located mitochondria were arranged vertically and had well-defined cristae. Some of basal mitochondria were elongated while others were oval in shape. Some of characteristic rough endoplasmic reticulum cisternae were noticed, but some fragmented rough endoplasmic reticulum were demonstrated as well (Figure 13c). Intercellular junctions were illustrated in many intercellular areas though, noticeably few areas were lacking intercellular junctions with obvious wide intercellular spaces (Figure 13d). Excretory duct cells revealed secretory granules delineated by definite membrane. Many granules were highly electron-dense but few had low electron-density. Mitochondria with characteristic cristae were observed. Rough endoplasmic reticulum with distinctive cisternae was noticed in some areas while, other areas showed fragmented rough endoplasmic reticulum. The intercellular junctions; junctional complexes and desmosomes were illustrated (Figure 13e). Goblet cells exhibited somewhat barrel shape. Their nuclei had condensed and loose chromatin and showed prominent nucleoli. Many secretory granules of moderate electron-density and high electron-density were observed. However, relatively few electron-lucent mucous secretory granules were demonstrated (Figure 13f).

Statistical results

Acini area%

Group I illustrated the highest mean area% of acini, the next was Group III, followed by Group IV and least mean value was demonstrated in Group II. High significant difference between studied groups was exemplified by One-way ANOVA test. Significant difference between each group when compared with the other groups was confirmed by Least Significant Difference post hoc test (Table 1, Figure 14).

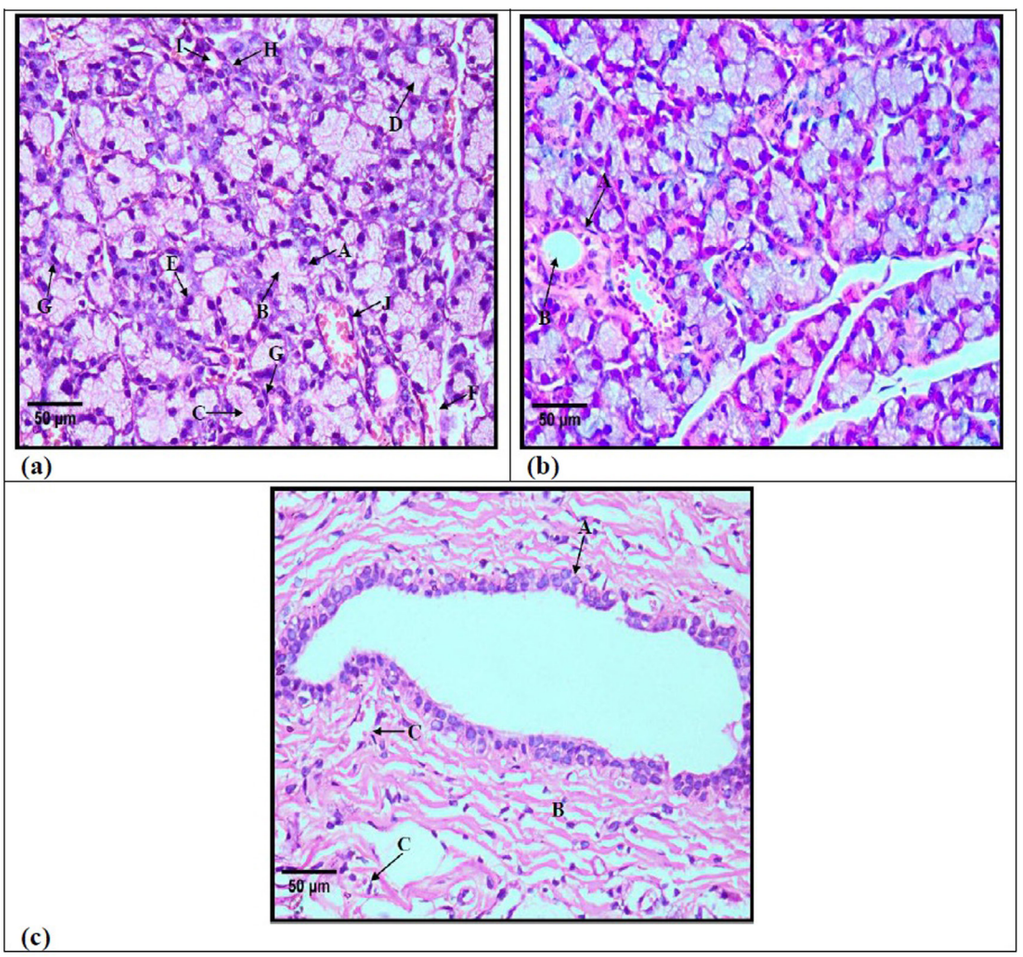

Fig. 1: Photomicrographs of Group I showing: (a): spherical serous acini formed of pyramidal cells (A). Cells' apices are eosinophilic (B) and surround apparently narrow lumen (C). Moderately basophilic cytoplasm (D). Spherical basal ap¬parently large nu¬clei (E). Connective tissue septa (F). Myoepi¬thelial cells' flattened nuclei (G). Intercalated duct cells with apparently large central rounded nuclei (H). Relatively large intercalated duct lumen (I). Blood vessels with normal endothelial lining (J). (b): striated duct is lined by columnar cells with eosinophilic cytoplasm, central nuclei and well-defined eosinophilic basal striations (A). Apparently regular and wide duct lumen (B). (c): obviously large excretory duct is lined by pseudostratified columnar epithelium and has lumen with variable diameter (A). Dense connective tissue with regular collagen fiber bundles (B). Blood vessels with normal endothelial lining (C), (H&E, original magnification x400).

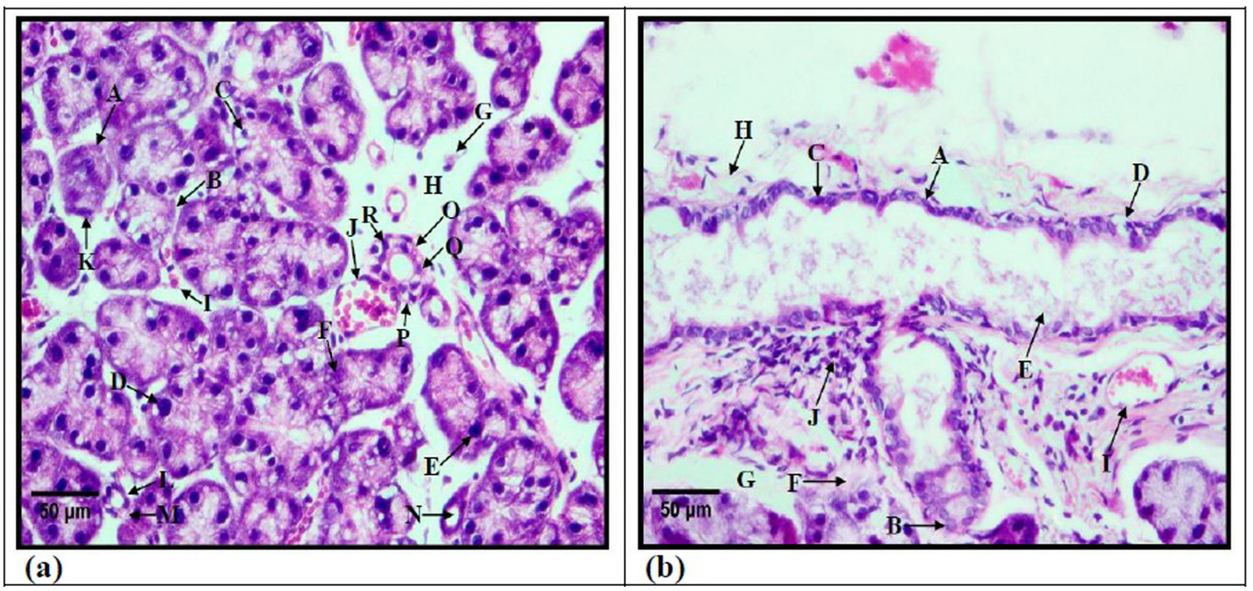

Fig. 2: Photomicrographs of Group II showing: (a): noticeably shrunken acini with perceptible decreased number. Some degenerated acini (A). Most of acini are distorted and show ill-defined cellular outline, loss of cytoplasmic basophilia, presence of cytoplasmic vacuolations and loss of cells' apices eosinophilia (B). Most cells have pyk¬notic (C), pleomorphic (D), hyperchromatic (E) and karyolitic nuclei (F). Desquamated cells among acini (G). Spacing between acini (H). Extravasated red blood cells (I). Congested blood vessels engorged with red blood cells (J). Pyknotic nuclei of myoepithelial cells (K). Intercalated duct cells show apparent loss of height, hyperchromatic and pyknotic nuclei as well as scanty cytoplasm (L). Some ductal cells have cytoplasmic vacuolations (M). Observable dilated duct lumen (N). Striated duct cells evidently lose both their height and basal striations (O) and have cytoplasmic vacuolations (P). Some duct nuclei are karyolitic (Q) and others are pyknotic and hyperchromatic (R). (b): excretory duct epithelial lining loses its pseudostratification (A). Most of ductal cells have karyolitic (B), hyperchromatic and pyknotic (C) nuclei. Some cells show cytoplasmic vacuolations (D). Stagnated secretion in lumen (E). Connective tissue shows areas of hyalinization (F), degeneration (G), disorganized collagen fiber bundles (H), dilated and congested blood vessels (I) as well as inflammatory cells infiltration (J), (H&E, original magnification x400).

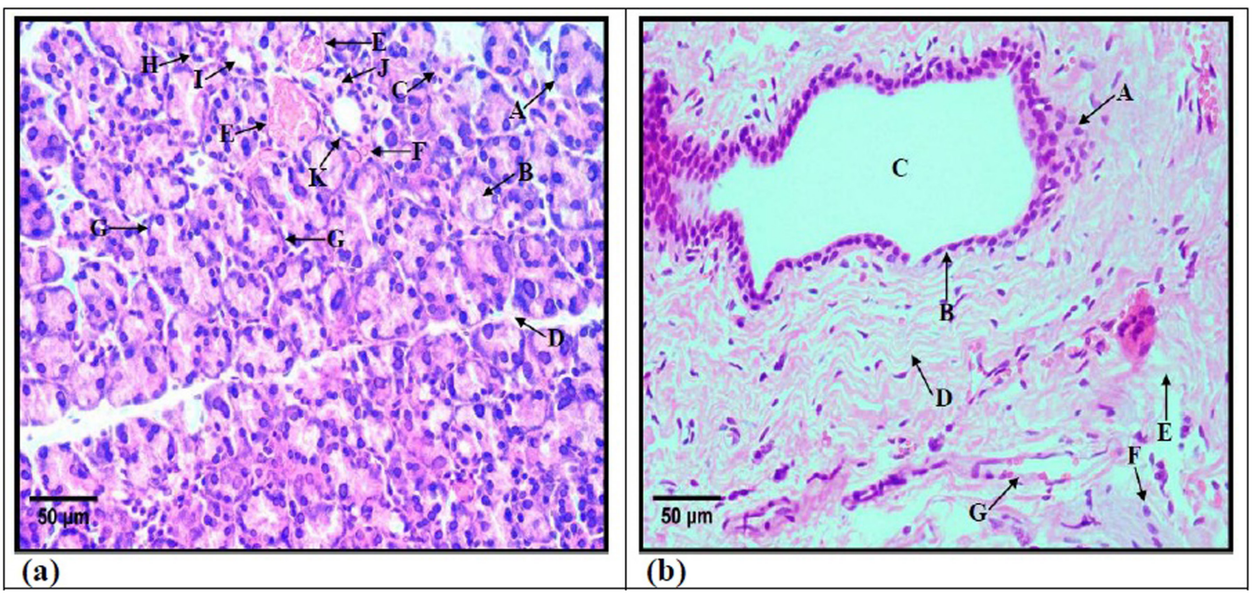

Fig. 3: Photomicrographs of Group III showing: (a): noticeably normal sized spherical acini composed of apparently high pyramidal cells with moderately basophilic cytoplasm and deeply stained basophilic rounded basal nuclei (A). Distinctly narrow acini lumen (B). Perceptibly very few degenerated acini (C). Connective tissue septa (D). Apparently large blood vessels (E). Markedly few extravasated red blood cells (F). Flattened nuclei of myoepi-thelial cells (G). Intercalated ducts are lined by cuboidal cells with basophilic cytoplasm and central apparently large spherical nuclei (H). Patently large ducts lumina compared to those of acini (I). Most of striated duct cells are columnar with central nuclei, acidophilic cytoplasm and eosinophilic basal striations (J). Obviously few ductal cells show apparent loss of both basal striations and cell height (K). (b): pseudostratified columnar epithelial lining of excretory duct (A). Manifestly few small areas show loss of pseudostratification (B). Apparently wide patent duct lumen (C). Regular collagen bundles of dense connective tissue (D). Apparently small areas of hyalinization (E). Markedly few scattered inflammatory cells (F). Blood vessels with normal endothelial lining (G), (H&E, original magnification x400).

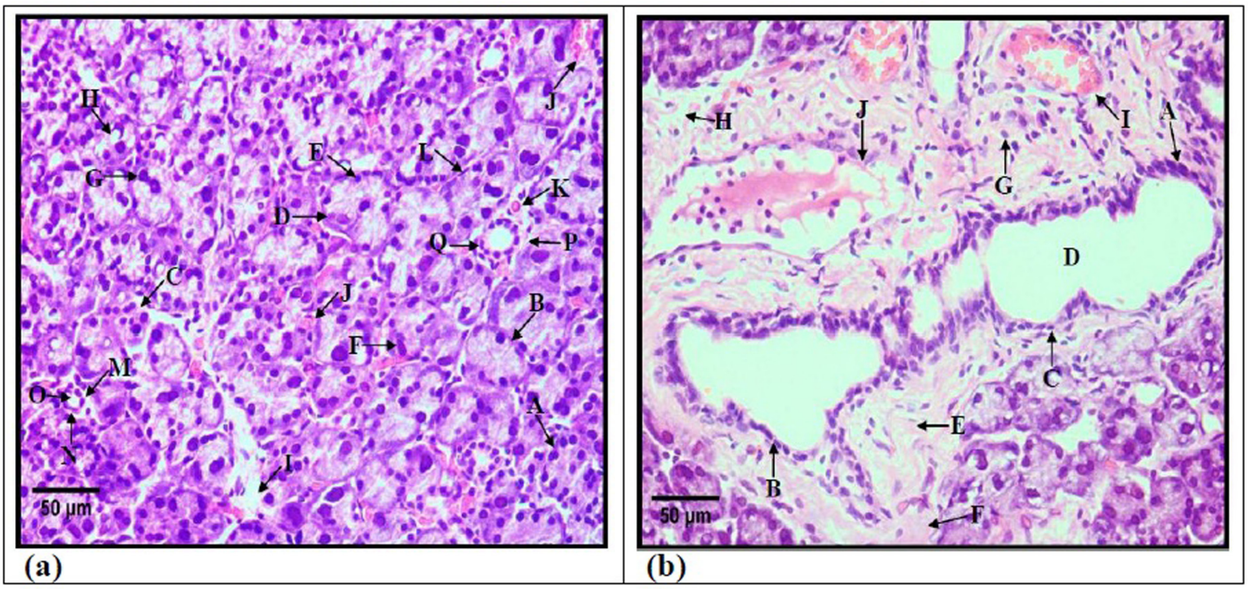

Fig. 4: Photomicrographs of Group IV showing: (a): most of acini are spherical in shape, strikingly normal sized and have conspicuously narrow lumen (A). Many of acinar cells are manifestly high pyramidal with basal deeply basophilic rounded nucleus and moderately basophilic cytoplasm (B). Apparently few acini seem to be shrunken with ill-defined cell outline (C). Some acinar cells have karyolitic (D), pyknotic (E), pleomorphic (F) and hyperchromatic (G) nuclei as well as cytoplasmic vacuolations (H). Discernibly small areas of degenerated connective tissue septa (I). Perceptibly small blood vessels (J) and extravasated red blood cells (K). Spindle shaped nuclei of myoepi¬thelial cells (L). Most of intercalated duct cells are cuboidal with distinctly large spherical nucleus and basophilic cytoplasm (M). Apparently few ductal cells are obviously reduced in height (N). The ducts' lumina are evidently larger than those of acini (O). Some of striated duct cells are columnar with basal eosinophilic striations, central nuclei and eosinophilic cytoplasm (P). Some cells of striated ducts show marked loss of height, loss of basal striations and pyknotic nuclei (Q). (b): some areas of excretory duct epithelial lining are pseudostratified columnar epithelium (A). Other areas show loss of pseudostratification (B). Apparently few pyknotic nuclei (C). Plainly wide and patent lumen (D). Areas of dense connective tissue show regularly arranged collagen bundles (E), areas of hyalinization (F), and inflammatory cells infiltration (G). Obviously small areas of degeneration (H). Blood vessels are congested and engorged by red blood cells (I). Dilated lymphatic vessels (J), (H&E, original magnification x400).

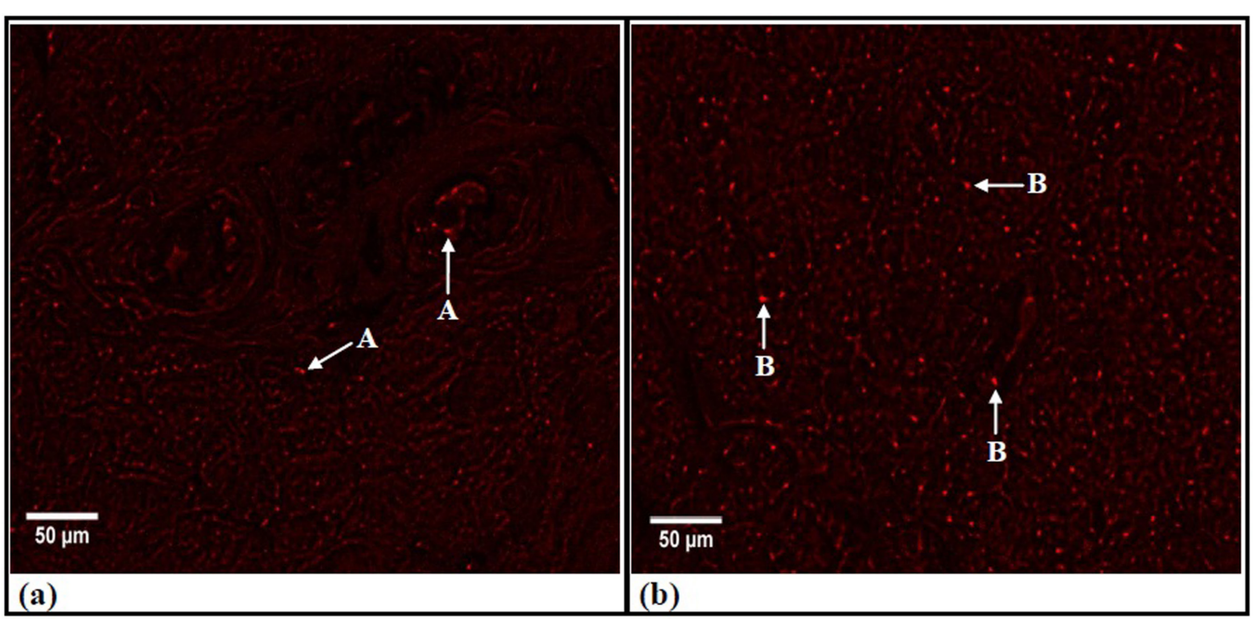

Fig. 5: Photomicrographs: (a)- Group III showing: some labeled-BM-MSCs (A). (b)- Group IV showing: obviously numerous labeled-BM-MSCs (B), (PKH26-fluorescence labeling, original magnification x400).

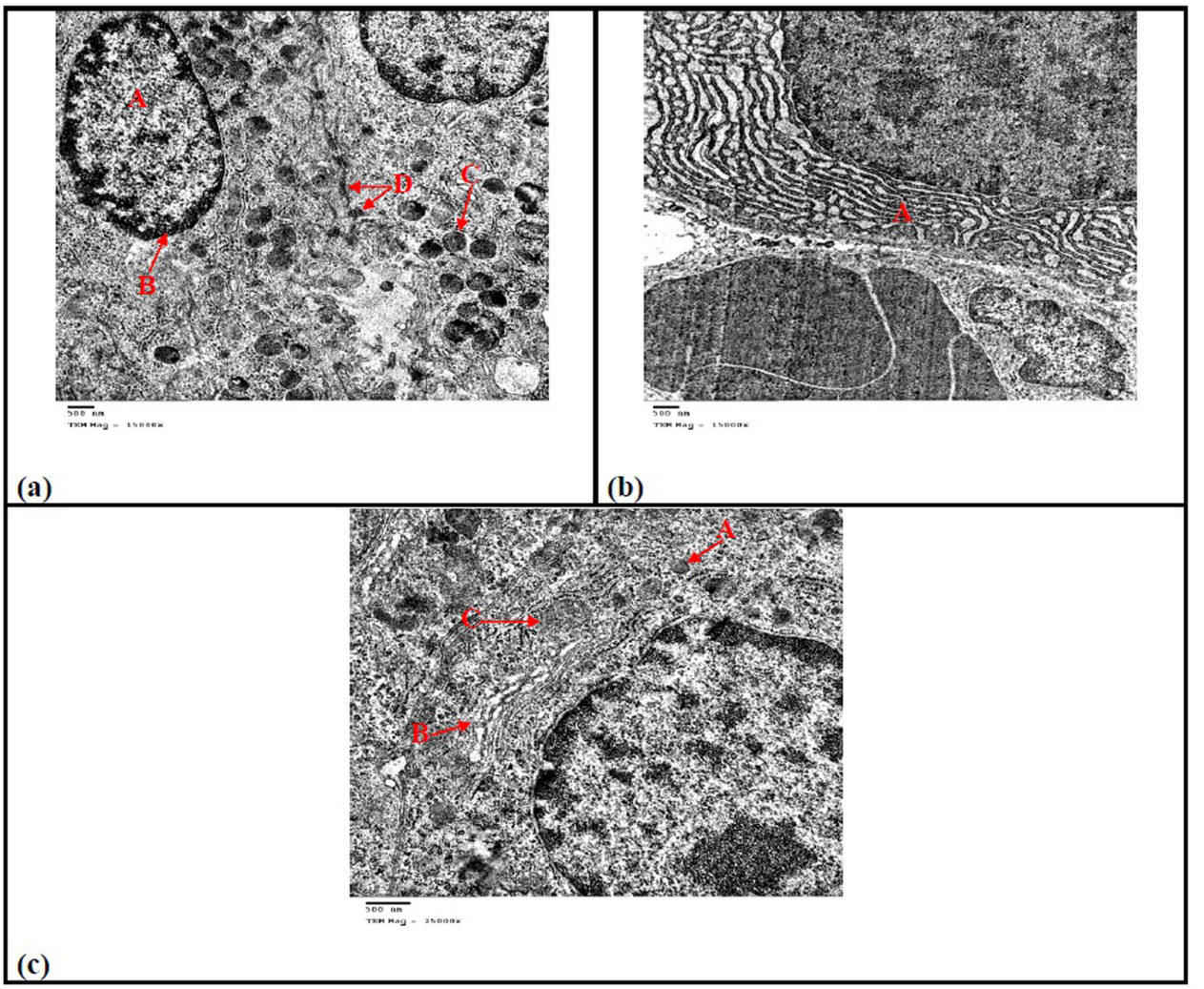

Fig. 6: Transmission electron micrographs of Group I acinar cells showing: (a)- Nucleus is apparently large with dispersed loose chromatin (A) and condensed chromatin attached to nuclear membrane (B). Apparently variable sized, spherical and highly electron-dense zymogen granules (C). Junctional complexes (D), (x15000). (b)- Basally arranged well-defined rough endoplasmic reticulum cisternae (A), (x15000). (c)- Zymogen granules are delineated by explicit membrane (A). Distinct Golgi complex saccules (B). Mitochondria with definite cristae (C), (x25000).

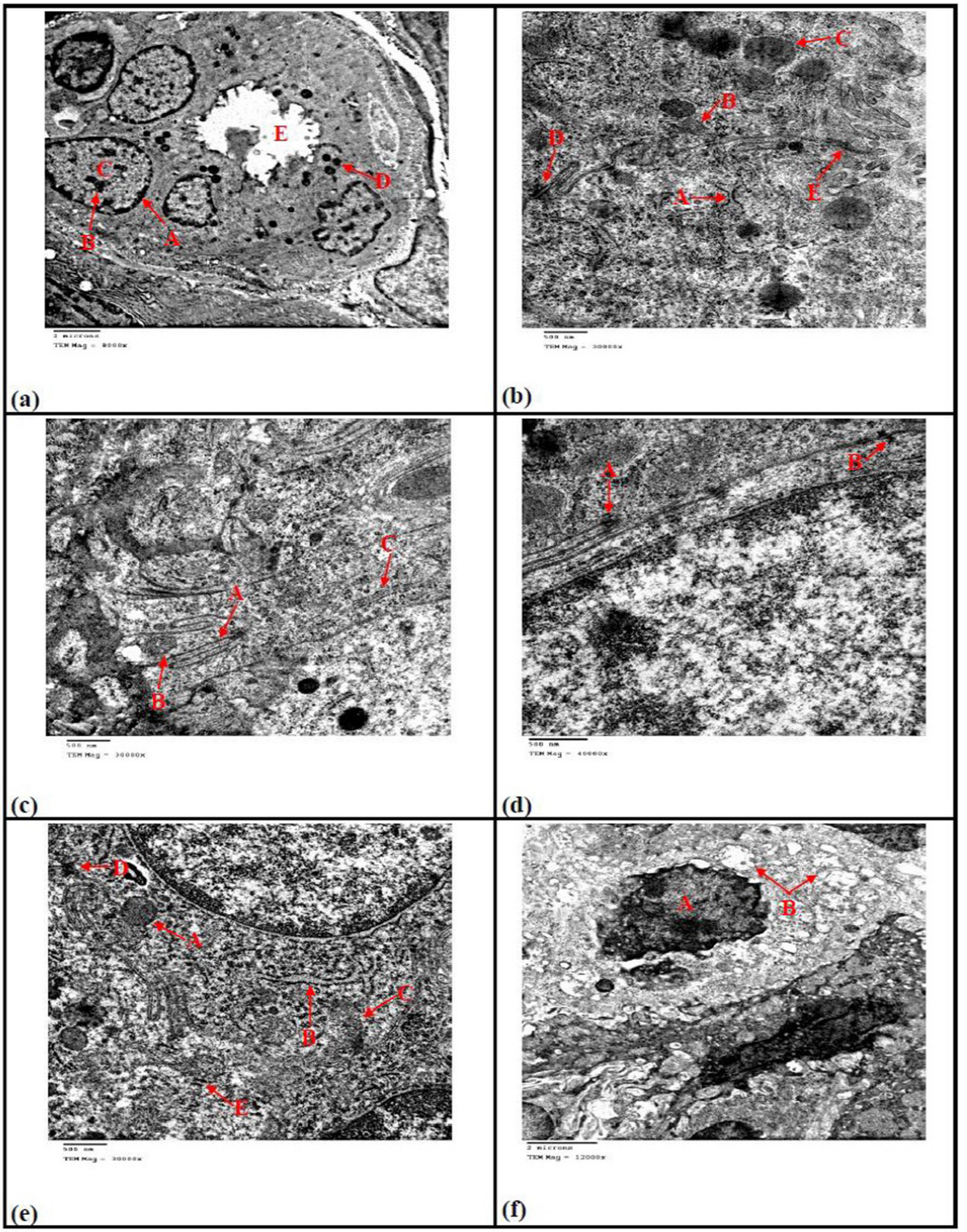

Fig. 7: Transmission electron micrographs of Group I: (a)- Intercalated duct cells showing: cuboidal cells have obviously large nuclei most of their condensed chromatin attached to nuclear membrane (A), some condensed chromatin (B) are dispersed within loose chromatin (C). Noticeably small highly electron-dense apical secretory granules (D). Regular duct lumen (E), (x8000). (b)- Intercalated duct cells showing: unambiguous rough endoplasmic reticulum cisternae (A). Mitochondria with remarkable cristae (B). Secretory granules are bounded by delineating membrane (C). Scattered desmosomes (D). Apical junctional complexes (E), (x30000). (c)- Striated duct cells showing: deeply folded basal plasma membrane (A). Alternating vertically arranged elongated mitochondria with well-defined cristae (B). Distinct cisternae of rough endoplasmic reticulum (C), (x30000). (d)- Striated duct cells showing: definite junctional complexes (A) and tight junctions (B), (x40000). (e)- Excretory duct cells showing: membrane bounded highly electron-dense secretory granules (A). Distinctive rough endoplasmic reticulum cisternae (B). Mitochondria with idiosyncratic cristae (C). Junctional complexes (D) and desmosomes (E), (x30000). (f)- Excretory duct cells showing: barrel shaped Goblet cell has nucleus with condensed chromatin (A) and electron-lucent mucous secretory granules (B), (x12000).

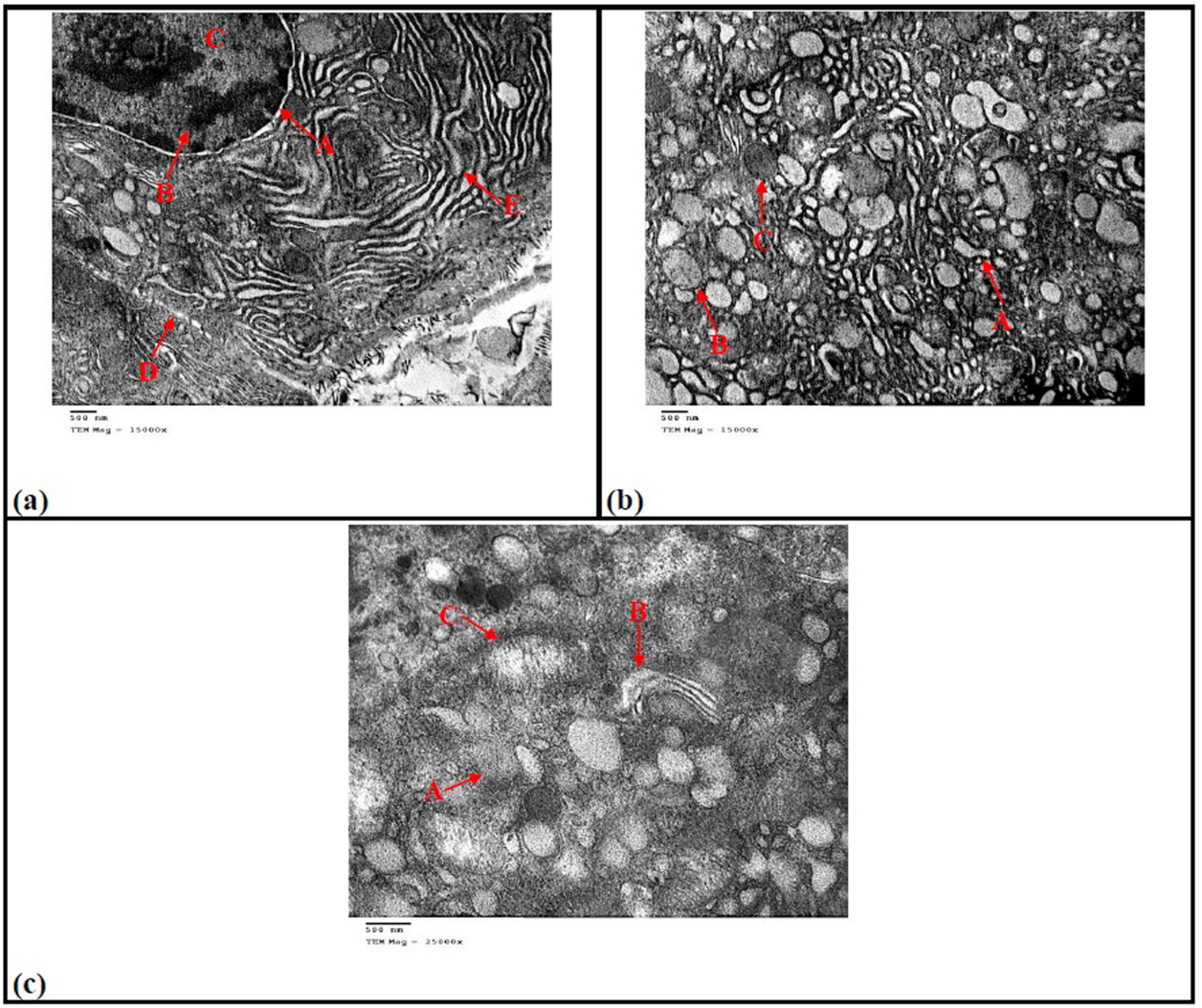

Fig. 8: Transmission electron micrographs of Group II acinar cells showing: (a)- Nuclei with condensed chromatin attached to nuclear membrane (A) and dispersed widely (B) within loose chromatin (C). Apparently widened intercellular canaliculi with loss of intercellular junctions (D). Areas of dilated rough endoplasmic reticulum cisternae (E), (x15000). (b)- Degenerated rough endoplasmic reticulum (A). Obvious different sized zymogen granules, most of granules have low electron-density (B). Noticeably few granules are moderately electron-dense (C), (x15000). (c)- Most of zymogen granules exhibit ill-defined membrane (A). Dilated saccules of Golgi apparatus (B). Degenerated swollen mitochondria with ill-defined cristae (C), (x25000).

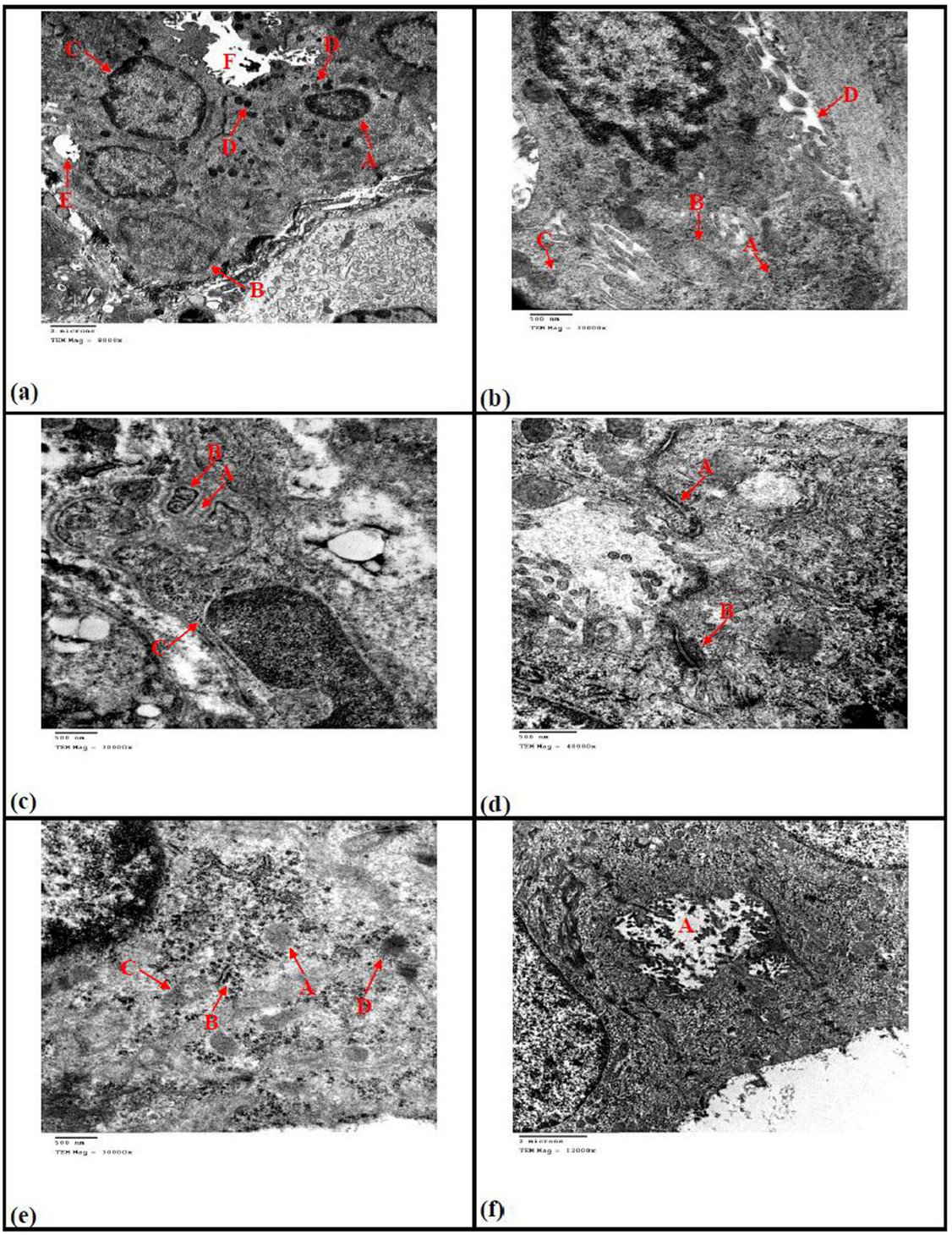

Fig. 9: Transmission electron micrographs of Group II: (a)- Intercalated duct cells showing: pyknotic (A), karyolitic (B) and irregular nuclei (C). Apparently few secretory granules with different electron densities (D). Perceptibly large cytoplasmic vacuolations (E). Irregular duct lumen (F), (x8000). (b)- Intercalated duct cells showing: fragmented rough endoplasmic reticulum (A). Degenerated mitochondria (B). Secretory granules lacked a definite bounding membrane (C). Lack of most intercellular junctions and noticeably wide intercellular spaces (D), (x30000). (c)- Striated duct cells showing: apparent loss of height and irregular outline. Very shallow basal plasma membrane infoldings (A) with apparently short degenerated mitochondria (B). Crumbled rough endoplasmic reticulum (C), (x30000). (d)- Striated duct cells showing: manifestly wide intercellular spaces (A). Evidently few intercellular junctions (B), (x40000). (e)- Excretory duct cells showing: low electron-dense secretory granules with ill-defined boundaries (A). Both rough endoplasmic reticulum (B) and mitochondria (C) are degenerated. Ill-defined intercellular junctions (D), (x30000). (f)- Excretory duct cells showing: Goblet cell has indistinct outline and devoid of mucous secretory granules. It shows karyolitic nucleus (A), (x12000).

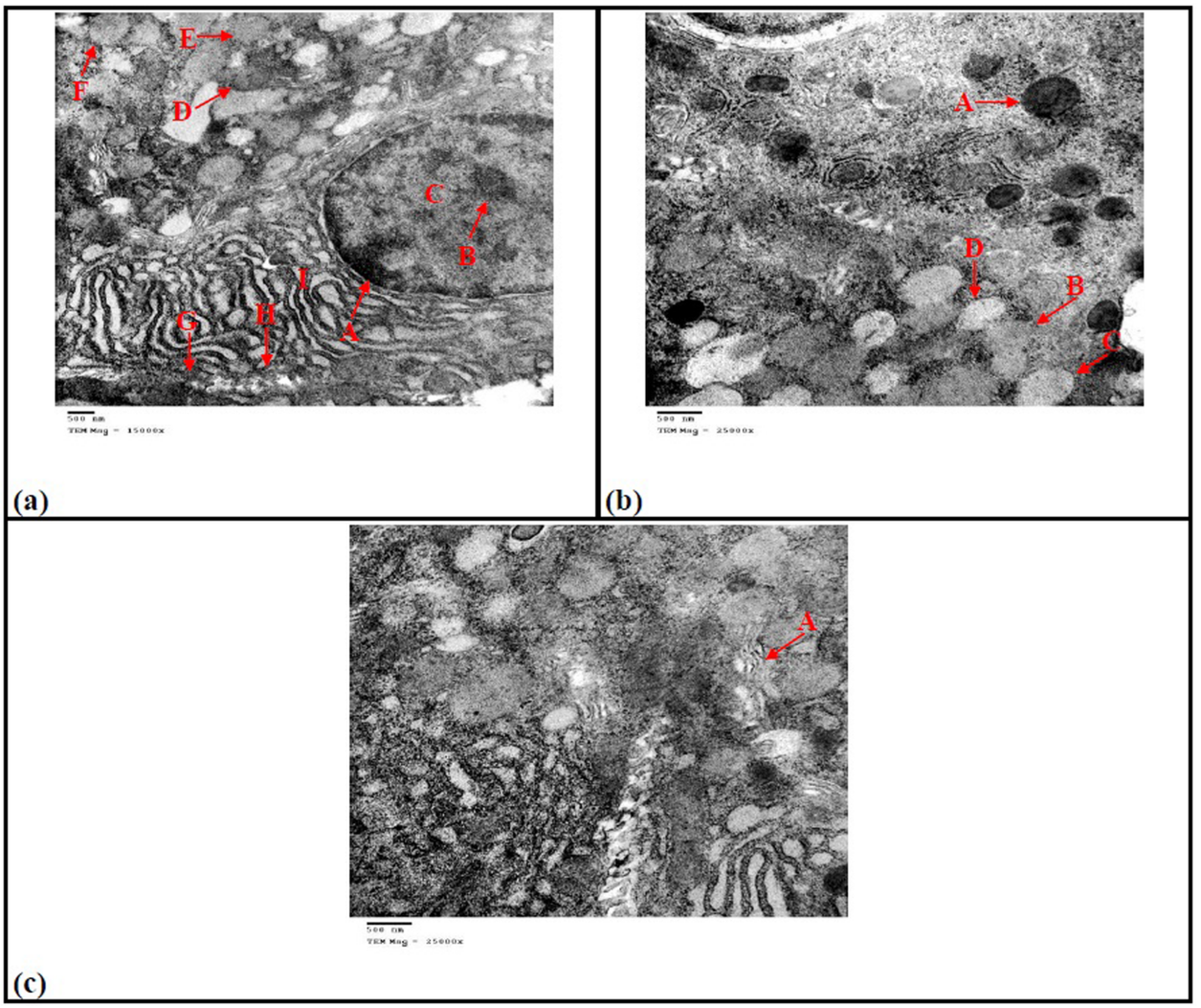

Fig. 10: Transmission electron micrographs of Group III acinar cells showing: (a)- Noticeably large nucleus with nuclear membrane has attached condensed chromatin (A) and prominent nucleoli (B) within dispersed loose chromatin (C). Spherical zymogen granules with apparent different sizes. Some granules show high electron-density (D). Other granules are moderately electron-dense (E) and few have low electron-density (F). Intercellular junctions in some areas (G). Absence of intercellular junctions in other areas with manifestly widened intercellular canaliculi (H). Basally arranged rough endoplasmic reticulum with well-defined cisternae (I), (x15000). (b)- Most of zymogen granules have well-defined boundaries and surrounded by recognizable membrane (A). Few granules exhibit ill-defined delineating membrane (B). Most of mitochondria have definite cristae (C). Few mitochondria are degenerated (D), (x25000). (c)- Characteristic flattened Golgi complex saccules (A), (x25000).

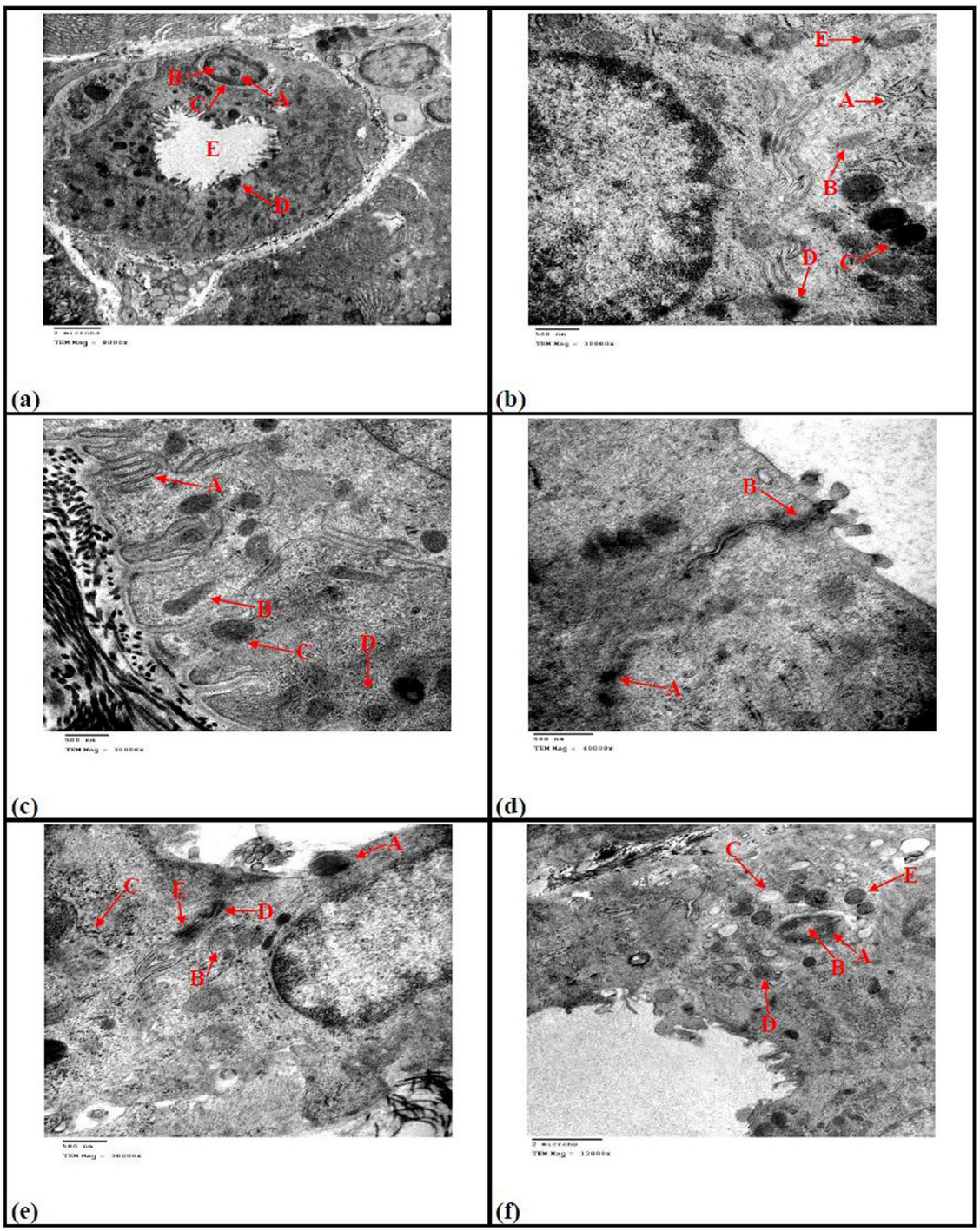

Fig. 11: Transmission electron micrographs of Group III: (a)- Intercalated duct cells showing: markedly large nuclei with prominent nucleoli (A) located within dispersed loose chromatin (B) and nuclear membrane shows attached condensed chromatin (C). Apparently variable sized highly electron-dense secretory granules are located apically (D). Almost regular duct lumen (E), (x8000). (b)- Intercalated duct cells showing: definite rough endoplasmic reticulum cisternae (A). Mitochondria with notable cristae (B). Secretory granules boundaries are demarcated by delineating membrane (C). Junctional complexes (D) and desmosomal junctions (E), (x30000). (c)- Striated duct cells showing: somewhat deep infoldings of basal plasma membrane (A) with alternating vertically arranged mitochondria which have well-defined cristae. Some of mitochondria are elongated (B). Other mitochondria are ovoid (C). Characteristic rough endoplasmic reticulum cisternae (D), (x30000). (d)- Striated duct cells showing: remarkable tight junctions (A) and junctional complexes (B), (x40000). (e)- Excretory duct cells showing: secretory granules with high electron-density and bordered by definite membrane (A). Mitochondria with distinctive cristae (B). Characteristic rough endoplasmic reticulum cisternae (C). Desmosomal junctions (D) and junctional complexes (E), (x30000). (f)- Excretory duct cells showing: barrel shaped Goblet cell has nucleus with both condensed (A) and loose chromatin (B). Some electron-lucent mucous secretory granules (C). Some secretory granules ranged from moderately (D) to highly electron-dense (E), (x12000).

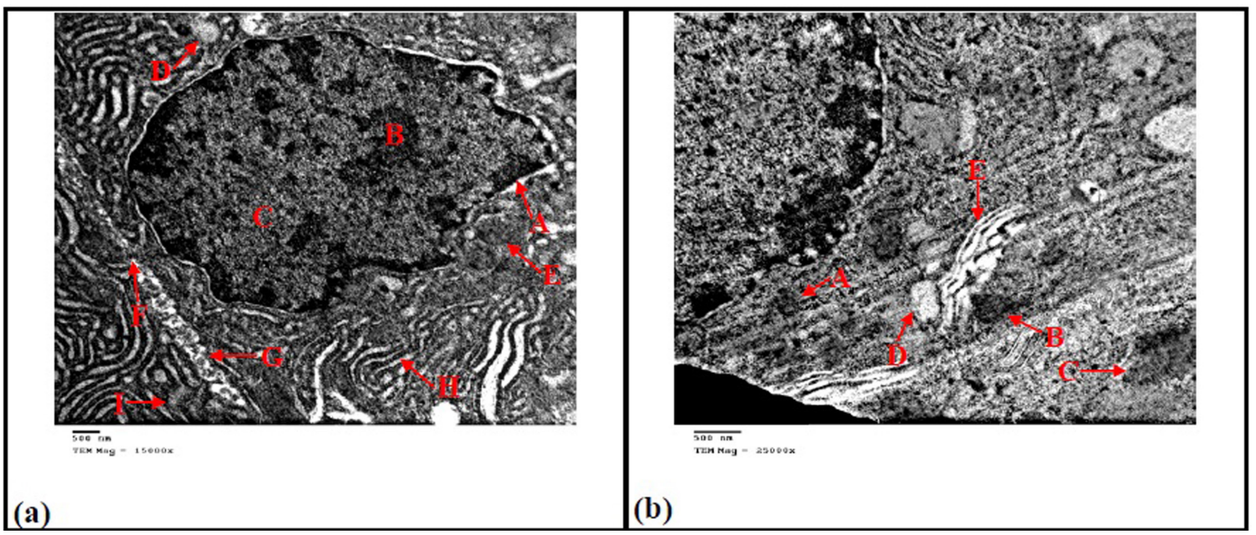

Fig. 12: Transmission electron micrographs of Group IV acinar cells showing: (a)- Apparently large nucleus with attached condensed chromatin to nuclear membrane (A) and prominent nucleoli (B) present in dispersed loose chromatin (C). Noticeably variable sizes of spherical zymogen granules. Some granules have low electron-density (D). Other granules are moderately electron-dense (E). Intercellular junctions in apparently few areas (F). Many areas are devoid of intercellular junctions with markedly widened intercellular canaliculi (G). Well-defined cisternae of rough endoplasmic reticulum are arranged basally (H). Apparently few areas show dilated cisternae (I), (x15000). (b)- Some zymogen granules display ill-defined bounding membrane (A). Other granules' boundaries are delineated by recognizable membrane (B). Some mitochondria show definite cristae (C). Other mitochondria are degenerated (D). Golgi apparatus saccules are flattened except for obviously few saccules that appear dilated (E), (x25000).

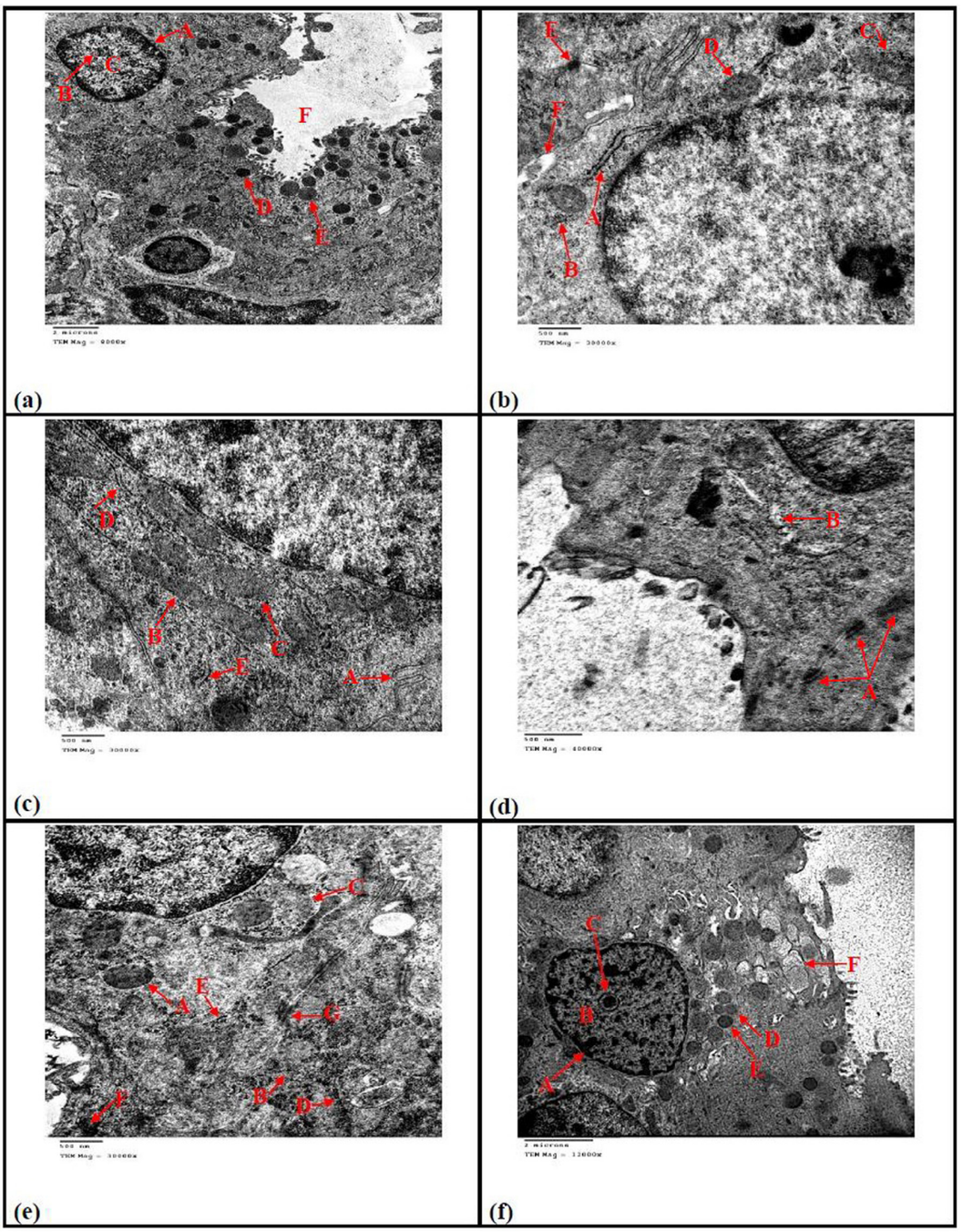

Fig. 13: Transmission electron micrographs of Group IV: (a)- Intercalated duct cells showing: obviously large nuclei with condensed chromatin attached to nuclear membrane (A) and prominent nucleoli (B) within dispersed loose chromatin (C). Noticeably variable sized secretory granules, some are highly electron-dense (D) while others have moderate electron-density (E). Somewhat irregular duct lumen (F), (x8000). (b)- Intercalated duct cells showing: rough endoplasmic reticulum with distinct cisternae (A) except, few cisternae are fragmented (B). Mitochondria with remarkable cristae (C). Membrane bounded secretory granules (D). Intercellular junctions in some areas (E). Other areas are devoid of intercellular junctions and show markedly wide intercellular spaces (F), (x30000). (c)- Striated duct cells showing: extremely shallow basal plasma membrane infoldings (A). Mitochondria are arranged vertically and have well-defined cristae. Some mitochondria are elongated (B) while others are oval (C). Some of characteristic rough endoplasmic reticulum cisternae (D). Some fragmented rough endoplasmic reticulum (E), (x30000). (d)- Striated duct cells showing: intercellular junctions in many areas (A). Noticeably few areas are lacking intercellular junctions with obvious wide intercellular spaces (B), (x40000). (e)- Excretory duct cells showing: secretory granules delineated by definite membrane, many granules are highly electron-dense (A) but few have low electron-density (B). Mitochondria with characteristic cristae (C). Rough endoplasmic reticulum with distinctive cisternae in some areas (D) but fragmented in other areas (E). Junctional complexes (F) and desmosomes (G), (x30000). (f)- Excretory duct cells showing: Goblet cell exhibits somewhat barrel shape. Its nucleus has condensed (A) and loose chromatin (B) and shows prominent nucleoli (C). Many secretory granules of moderate electron-density (D) and high electron-density (E). Relatively few electron-lucent mucous secretory granules (F), (x12000).

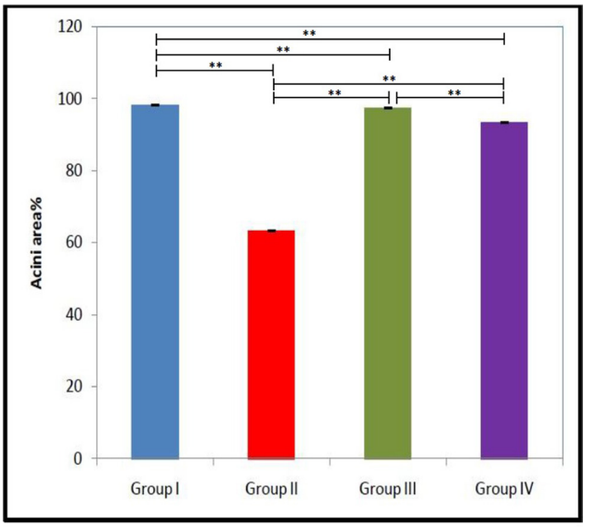

Fig. 14: Bar chart of results representing means and SD values of acini area% in all studied groups. ***P* <0.001 between groups as shown

Table 1: Showing the mean ± SD values, the range values, results of ANOVA and Least Significant Difference post hoc tests for the comparison between different studied groups regarding acini area%

Acini area%	Group I	Group II	Group III	Group IV	ANOVA	*p-value*
Mean±SD	98.19±0.09	63.29±0.09[a]	97.41±0.09[ab]	93.31±0.09[abc]	36.478	<0.001**
Range	98.1-98.3	63.2-63.4	97.3-97.5	93.2-93.4		

Superscript letters indicate; a: significant difference with Group I; b: significant difference with Group II; c: significant difference with Group III according to Least Significant Difference post hoc test.
**: Highly significant at *p-value* <0.001

DISCUSSION

Carbimazole might affect the cells of the parotid gland by depleting the first line of enzymatic antioxidant defense (glutathione peroxidase, catalase and superoxide dismutase) which leads to oxidative stress production that eventually ends up by cellular damage[6,22].

BM-MSCs have beneficial effects on regeneration of salivary glands by differentiation into salivary gland cells and increasing density of microvessels. In addition, they are resistible to the deleterious effects of hypoxia and oxidative stress[11,23].

Male albino rats were utilized in current study to avoid female's hormonal effect[24].

Since parotid gland presents aerobic metabolism mainly thus, it is more susceptible to oxidative damage[3].

Standard histological features of parotid gland and statistical results of its acini area% stated in Group I results of this study are in line with those of previous investigators[18].

In present study, the deleterious histological changes and statistical results of acini area% reported in Group II results could be ascribed to effect of carbimazole that causes generation and flux of superoxide radicals during aerobic metabolism. These radicals consequently lead to diminution of antioxidant enzymes activities that accordingly leads to accumulation of hydrogen peroxide and superoxide radicals and so production of oxidative stress. Interruption of cell's DNA, peroxidation of lipids, protein carbonylation and nitration in addition to destruction of phospholipids "main constituent of all cell membranes" are consequences of carbimazole-induced oxidative stress that lead to destruction of cells and organs. Moreover, cellular tumor antigen p53 plays a role in arresting cell cycle and its level increases as a reaction to DNA damage during oxidative stress which leads to enhancement of cell apoptosis. Additionally, mononuclear inflammatory infiltrate is a result of pro-inflammatory cytokines formation under influence of tumor necrosis factor alpha during oxidative stress condition[6,7,22,25].

Group III results herein in this study illustrated almost normal both histological features and acini area%. This could be attributed to maintenance of BM-MSCs for their stemness via activation of cellular tumor antigen p53 under influence of oxidative stress condition where p53 binds to the promoters of self-renewal in BM-MSCs and possesses its stemness role[25,26]. Also, BM-MSCs have paracrine proliferative/pro-survival effects on remaining salivary stem cells present in surrounding environment. Beside, BM-MSCs down regulate production of both reactive oxygen species and the persuasive inflammatory molecule "interferon-gamma" in concomitance with secretion of anti-inflammatory mediators, antioxidants and growth factors that consequently lead to improvement of cell survival, immune modulation and angiogenesis.

Thus, BM-MSCs contribute in regeneration and repair of salivary glands[11,27-31]. It was reported that BM-MSCs were integrated and differentiated into salivary gland cells such that the treated gland tissue became comparable to the normal control tissue after 43 days of treatment by BM-MSCs. The previous fact could explain also the fluorescence labeling results of Group III in present research where the labeled-BM-MSCs seemed to be reduced because, the fluorescent molecules become insufficient as the cells divide and differentiate[20,32-34].

Although histological results and statistical results of acini area% of Group IV in the current study demonstrated reparative features and improvement however, some of degenerative signs were persisted. This could be ascribed to the fact that about half of BM-MSCs differentiated into salivary gland cells after 3 weeks of their administration which significantly contributes in regeneration of salivary glands. However, the complete salivary glands regeneration is achieved by differentiation of all BM-MSCs which accomplished after 6 weeks of their application. The previous information explains as well the fluorescence labeling results of Group IV in this study as the obviously numerous labeled-BM-MSCs noticed could be due to presence of sufficient fluorescent molecules as long as the cells remain undifferentiated and undivided[20,32,34].

Normal ultra-structure features recorded in Group I results herein in this study are in agreement with those of previous investigators[35,36].

In the current research, ultra-structure results of Group II could be attributed to the effect of free radicals produced after treatment by carbimazole which in return created oxidative stress condition that causes damage to the cell membrane, intercellular junctions and DNA, affects the cells' nuclei as well as all cells' organelles specially mitochondria which play an important role in mediating cell death. Carbimazole increases the permeability of mitochondrial membrane which results in release of apoptogenic factors into cell's cytoplasm that enhance cell apoptosis and necrosis ending by cell death. Degeneration of mitochondria leads to deficient adenosine triphosphate and consequently insufficient energy which contributes in degeneration of the different organelles and thus appearance of autophagic vacuoles as well[6,7,22]. Reactive oxygen species not only attack the lipids and proteins forming the membrane of different secretory granules leading to its damage but also they interact with nucleic acids and proteins present in zymogen granules as well as other secretory granules and causing impairment in their stability[37,38].

Ultra-structure results of Group III in this research could be ascribed to different effects of BM-MSCs. The BM-MSCs not only capable to differentiate into different types of salivary gland cells to replace the degenerated ones but also "through their paracrine effects" they can release bioactive components called “soup” such as growth factors and chemokines that remodel the microenvironment. Remodeling of microenvironment by “soup” occurs through vasculogeneic, anti-inflammatory, pro-proliferative, and anti-apoptotic cues. Also, BM-MSCs rescue affected cells by transferring cellular materials including large organelles from them to targeted recipient cells through membrane channels "tunneling nanotubes". In particular, intercellular transfer of mitochondria through previously mentioned channels contributes to a great extent in increasing cell viability. Moreover, BM-MSCs display potent antioxi-dant effects which have protective role against carbimazole-induced oxidative stress[11,39,40].

Though ultra-structure results of Group IV in current research illustrated reparative signs however, some degenerative features were recorded. This could be referred to the duration of treatment by BM-MSCs in which only half of BM-MSCs become differentiated after 3 weeks of their application, while differentiation of all BM-MSCs is achieved after 6 weeks of their administration[32,34].

Further investigations are required to evaluate the possible prophylactic role of BM-MSCs application before carbimazole administration.

CONCLUSIONS

Carbimazole causes damage to structure of parotid salivary glands. The potency of BM-MSCs in regeneration of parotid salivary glands and improvement of carbimazole-induced degenerative changes is time dependent.

Oral hygiene monitoring in patients undergoing carbimazole treatment is essential. BM-MSCs remedy is promising for treatment of degenerative salivary glands disorders.

CONFLICT OF INTERESTS

There are no conflicts of interest.

REFERENCES

1. Estecondo S, Codon S and Casanave E: Histological study of the salivary glands in Zaedyus pichiy (Mammalia, Xenarthra, Dasypodidae). Int. J. Morphol. (2005) 23(1): 19-24.

2. Delporte C, Bryla A and Perret J: Aquaporins in salivary glands: from basic research to clinical applications. Int. J. Mol. Sci. (2016) 17(2): 1-13.

3. Garbowska M, Lukaszuk B, Miklosz A, Wroblewski I, Kurek K, Ostrowska L, Chabowski A, Zendzian-Piotrowska M and Zalewska A: Sphingolipids metabo¬lism in the salivary glands of rats with obesity and strepto¬zotocin induced diabetes. J. Cell Physiol. (2017) 232(10): 2766–2775.

4. Sakr SA, Mahran HA and Nofal AE: Effect of selenium on carbimazole induced histopathological and histochemical alterations in prostate in albino rats. American J. of Medicine and Medical Science. (2012) 2(1): 5-11.

5. Choi J and Jee JG: Repositioning of thiourea-containing drugs as tyrosinase inhibitors. Int. J. Mol. Sci. (2015) 16(12): 28534-28548.
6. Sakr SA, Abdel-Ghafar FR and Abo-El-Yazid SM: Selenium ameliorates carbimazole induced hepatotoxicity and oxidative stress in albino rats. Journal of Coastal Life Medicine. (2015) 3(2): 139-145.
7. Bashandy MA: Role of rosemary (Rosmarinus officinalis) extract on carbimazole induced alteration in pancreas of adult male albino rat (histological, immuno-histochemical and ultrastructural study). Journal of American Science. (2018) 14(1): 110-124.
8. Prasanchd K and Devi R: Stem cells-a revolution in regeneration of the periodontium: a review article. Journal of Academy of Dental Education. (2018) 4(2): 7–11.
9. Sumita Y, Liu Y, Khalili S, Maria OM, Xia D, Key S, Cotrim AP, Mezey E and Tran SD: Bone marrow-derived cells rescue salivary gland function in mice with head and neck irradiation. Int. J. Biochem. Cell Biol. (2011) 43(1): 80–87.
10. Wang Y, Zhou L, Li C, Xie H, Lu Y, Wu Y and Liu H: Bone marrow-derived cells homing for self-repair of periodontal tissues: a histological characterization and expression analysis. Int. J. Clin. Exp. Pathol. (2015) 8(10): 12379-12389.
11. Lombaert I, Movahednia MM, Adine C and Ferreira JN: Concise review: salivary gland regeneration: therapeutic approaches from stem cells to tissue organoids. Stem Cells. (2017) 35(1): 97–105.
12. Abdel Aziz M, Atta H, Mahfouz S, Fouad H, Roshdy N, Ahmed H, Rashed L, Sabry D, Hassouna A and Hasan N: Therapeutic potential of bone marrow-derived mesenchymal stem cells on experimental liver fibrosis. Clin. Biochem. (2007) 40(12): 893-899.
13. Fikry H, Abdel Gawad S and Baher W: Therapeutic potential of bone marrow derived mesenchymal stem cells on experimental liver injury induced by Schistosoma mansoni: a histological Study. International Journal of Stem Cells. (2016) 9(1): 96–106.
14. Elsaadany B, El Kholy S, El Rouby D, Rashed L and Shouman T: Effect of transplantation of bone marrow derived mesenchymal stem cells and platelets rich plasma on experimental model of radiation induced oral mucosal injury in albino rats. International Journal of Dentistry. (2017) 2017: 1-9.
15. Nampoothiri M, John J, Kumar N, Mudgal J, Nampurath G and Chamallamudi M: Modulatory role of simvastatin against aluminium chloride-induced behavioural and biochemical changes in rats. Behavioural Neurology. (2015) 2015: 1–9.
16. Sakr SA, Hassab ELnab SE, Okdah YA and El-Shabka AM: Impact of ginger aqueous extract on carbimazole induced testicular degenerative alterations and oxidative stress in albino rats. Journal of Coastal Life Medicine. (2017) 5(4): 167-173.
17. Shredah M and El-Sakhawy M: Immunohistochemical expression of activated caspase-3 in the parotid salivary glands of rats after long administration of Myristica fragrans. International Journal of Advanced Research. (2014) 2(12): 493–499.
18. Ramadan E, Hegab A, Hussein Y and Abdul Rahman M: Postnatal developmental changes of the parotid gland in albino rats: histological, immunohistochemical and morphometric study. British J. Sci. (2014) 11(2): 1-15.
19. Bancroft JD and Layton C: Bancroft's theory and practice of histological techniques (7th ed.). Churchill Livingstone: Elsevier (2013) pp: 173-186.
20. Yuan L, Liu H and Wu M: Human embryonic mesenchymal stem cells participate in differentiation of renal tubular cells in newborn mice. Experimental and Therapeutic Medicine. (2016) 12(2): 641-648.
21. Mohsen R, Halawa A and Hassan R: Role of bone marrow-derived stem cells versus insulin on filiform and fungiform papillae of diabetic albino rats (light, fluorescent and scanning electron microscopic study). Acta Histochemica. (2019) 121(7): 812-822.
22. Al-Amoudi WM, Mahboub FA, Lamfon HA and Lamfon NA: Assessing induced effect of curcumin on methimazole hepatic damage in albino rats: a histological and histochemical study. Canadian Journal of Pure and Applied Sciences. (2016) 10(3): 3961-3969.
23. El-Badawy A, Amer M, Abdelbaset R, Sherif SN, Abo-Elela M, Ghallab YH, Abdelhamid H, Ismail Y and El-Badri N: Adipose stem cells display higher regenerative capacities and more adaptable electro-kinetic properties compared to bone marrow-derived mesenchymal stromal cells. Scientific Reports. (2016) 6: 1-11.
24. Souza MF, Couto-Pereira NS, Freese L, Costa PA, Caletti G, Bisognin KM, Nin MS, Gomez R and Barros HMT: Behavioral effects of endogenous or exogenous estradiol and progesterone on cocaine sensitization in female rats. Brazilian Journal of Medical and Biological Research. (2014) 47(6): 505-514.
25. Olivos II DJ and Mayo LD: Emerging non-canonical functions and regulation by p53: p53 and stemness. Int. J. Mol. Sci. (2016) 17(12): 1-30.
26. Katagiri H, Kushida Y, Nojima M, Kuroda Y, Wakao S, Ishida K, *et al*: A Distinct subpopulation of bone marrow mesenchymal stem cells, muse cells, directly commit to the replacement of liver components. Am. J. Transplant. (2016) 16(2): 468–483.

27. Chen L, Tredget EE, Wu PY and Wu Y: Paracrine factors of mesenchymal stem cells recruit macrophages and endothelial lineage cells and enhance wound healing. PLoS ONE. (2008) 3(4): 1-12.

28. Iyer SS and Rojas M: Anti-inflammatory effects of mesenchymal stem cells: novel concept for future therapies. Expert Opin. Biol. Ther. (2008) 8(5): 569–581.

29. Uccelli A, Moretta L and Pistoia V: Mesenchymal stem cells in health and disease. Nat. Rev. Immunol. (2008) 8(9): 726–736.

30. Mumaw JL, Schmiedt CW, Breidling S, Sigmund A, Norton NA, Thoreson M, Peroni JF and Hurley DJ: Feline mesenchymal stem cells and supernatant inhibit reactive oxygen species production in cultured feline neutrophils. Res. Vet. Sci. (2015) 103: 60-69.

31. Denewar M and Amin L: Role of bone marrow-derived mesenchymal stem cells on the parotid glands of streptozotocin induced diabetes rats. Journal of Oral Biology and Craniofacial Research. (2020) 10(2020): 33–37.

32. Lin CY, Chang FH, Chen CY, Huang CY, Hu FC, Huang WK, Ju SS and Chen MH: Cell therapy for salivary gland regeneration. J. Dent. Res. (2011) 90(3): 341–346.

33. Lim JY, Yi T, Choi JS, Jang YH, Lee S, Kim HJ, Song SU and Kim YM: Intraglandular transplantation of bone marrow-derived clonal mesenchymal stem cells for amelioration of post-irradiation salivary gland damage. Oral Oncol. (2013) 49(2): 136–143.

34. Yoo C, Vines JB, Alexander G, Murdock K, Hwang P and Jun H: Adult stem cells and tissue engineering strategies for salivary gland regeneration: a review. Biomaterials Research. (2014) 18(9): 1-12.

35. Tandler B, Pinkstaff CA and Phillips CJ: Interlobular excretory ducts of mammalian salivary glands: structural and histochemical review. The Anatomical Record Part A. (2006) 288(5): 498–526.

36. Hamza SA, Aly HM, Soliman SO and Abdallah DM: Ultrastructural study of the effect of zinc oxide nanoparticles on rat parotid salivary glands and the protective role of quercetin. Alexandria Dental Journal. (2016) 41(3): 232-237.

37. Frisard M and Ravussin E: Energy metabolism and oxidative stress: impact on the metabolic syndrome and the aging process. Endocrine. (2006) 29(1): 27–32.

38. Witt H, Apte M, Keim V and Wilson J: Chronic pancreatitis: challenges and advances in pathogenesis, genetics, diagnosis, and therapy. Gastroenterology. (2007) 132(4): 1557-1573.

39. Liu Z, Hu G, Luo X, Yin B, Shu B, Guan J and Jia C: Potential of bone marrow mesenchymal stem cells in rejuvenation of the aged skin of rats. Biomedical Reports. (2017) 6(3): 279-284.

40. Naji A, Favier B, Deschaseaux F, Rouas-Freiss N, Eitoku M and Suganuma N: Mesenchymal stem/stromal cell function in modulating cell death. Stem Cell Research & Therapy. (2019) 10(56): 1-12.

الملخص العربى

التقييم الهيستولوجى، المادة المشعة و التركيب الدقيق للتأثير المحتمل للعلاج بالكاربيمازول و اعطائه مع الخلايا الجذعية الوسيطة المشتقة من نخاع العظم على الغدد النكافية للجرذان البيضاء

إسراء جمال حسن[١]، هبه العدوى[٢]، أمانى أحمد ربيع[١]

[١]قسم بيولوجيا الفم – كلية طب الفم والأسنان - جامعة المستقبل فى مصر- القاهرة-مصر.

[٢]قسم بيولوجيا الفم-كليه طب الأسنان (للبنات)-جامعه الأزهر- القاهرة-مصر.

المقدمة: الكاربيمازول دواء شائع لعلاج فرط نشاط الغدة الدرقية. ولقد وجد ان له العديد من الآثار الجانبية على الأنسجة المختلفة. تعتبر الخلايا الجذعية الوسيطة المشتقة من نخاع العظم فعالة في تجديد الأنسجة.

الهدف: تقييم نتيجة تناول الكاربيمازول (عقار مضاد للغدة الدرقية) على بنية الغدة النكافية للجرذان البيضاء والنتيجة المحتمله لتطبيق الخلايا الجذعية الوسيطة المشتقة من نخاع العظم على فترات مختلفة.

مواد و طرق الدراسة: تم استخدام أربعين من ذكور الجرذان البيضاء البالغة و تقسيمهم إلى: المجموعة الأولى: اعطيت الجرذان الماء المقطر. المجموعة الثانية: اعطيت الجرذان الجرعة العلاجية من الكاربيمازول. المجموعة الثالثة: تلقت الجرذان الكاربيمازول وجرعة وحيدة من الخلايا الجذعية الوسيطة المشتقة من نخاع العظم في بداية التجربة. المجموعة الرابعة: تلقت الجرذان الجرعة العلاجية من الكاربيمازول وبنهاية الأسبوع الثالث تم حقن الجرذان مرة واحدة بالخلايا الجذعية الوسيطة المشتقة من نخاع العظم. تم تحضير العينات للفحص بواسطة المجهر الضوئى، مجهر المواد المشعة، و المجهر الإلكتروني النافذ. تم التحليل الاحصائى لبيانات التحليل النسيجي للنسبة المئوية لمساحة العنيبات باستخدام تحليل التباين.

النتائج: أوضحت كل من الفحوصات النسيجية والبنية التحتية أن الغدة النكافية لها بنية طبيعية في المجموعة الأولى وكانت طبيعية تقريبًا في المجموعة الثالثة. أظهرت المجموعة الثانية عنيبات ونظام قنوات مشوه. أظهرت المجموعة الرابعة خصائص طبيعية في بعض العنيبات وبعض مناطق نظام القنوات و مظاهر تنكسية في مناطق أخرى. اظهر الفحص باستخدام مادة مشعة وجود بعض الخلايا الجذعية الوسيطة المشتقة من نخاع العظم في المجموعة الثالثة و كان عدد الخلايا اكثر في المجموعة الرابعة. أظهرت النتائج الإحصائية أعلى متوسط لمساحة العنيبات المئوية في المجموعة الأولى ، ثم المجموعة الثالثة ، ثم المجموعة الرابعة ، تليها المجموعة الثانية.

الاستنتاج: الكاربيمازول له تأثيرات متلفة على انسجة الغدة النكافية للجرذان البيضاء. تعمل الخلايا الجذعية الوسيطة المشتقة من نخاع العظم على تحسين التأثيرات الضارة للكاربيمازول بتناسب طردى مع عامل الوقت.